Analysis of Active Damping of a Silicon Microphone Using a Linear Controller

Jinli Qu, N. Eva Wu, Ronald N. Miles, and Henik Vargas

Abstract—**This paper presents a model of a silicon microphone with active electronic damping. The microphone has low passive damping to minimize thermal noise, and employs active damping from electrostatic actuation to improve its dynamic performance. To apply the linear robust control approach, the nonlinear dynamic system is modeled as a linear system with bounded parameters, and a controller is designed using the H_∞ method which successfully drives the electrostatic actuator to generate the desired active damping. The effectiveness of the controller has been verified through simulation in both frequency and time domains.**

I. INTRODUCTION

SILICON microphones have significant potential for achieving improved performance over conventional microphone designs with smaller size and lower cost. These performance improvements will be possible when researchers are able to fully take advantage of the unique capabilities of microfabricated devices. The possibility of implementing electronic force-feedback has been utilized in many micromachined sensors to provide significant performance improvements [1]. This approach has, however, not been adequately taken advantage of to achieve performance improvements in silicon microphones. A primary aim of the present study is to examine the possibility of performance improvement of a novel directional microphone concept that is very well-suited to an electronic force-feedback scheme.

A typical transfer function for a silicon microphone takes the form $\dfrac{1}{ms^2 + cs + k}$, where m, c, and k are the microphone's mass, damping coefficient, and stiffness, respectively and s is the Laplace transform variable. A major trade-off in microphone design comes from the choice of the system's damping coefficient c. According to the equipartion theorem and the Nyquist relation, the microphone's thermal noise is determined by its damping

Jinli Qu and Ronald Miles are with the Dep. Of Mechanical Engineering, Binghamton University, PO Box 6000, Binghamton, NY, 13902 (e-mail: jqu1@binghamton.edu, miles@binghamton.edu)
N. Eva Wu and Henik Vargas are with the Dep. Of Electrical & Computer Engineering, Binghamton University, Binghamton University, PO Box 6000, Binghamton, NY, 13902 (e-mail: evawu@binghamton.edu,)
.

coefficient [2]. More damping produces more thermal noise relative to the detected input sound pressure. In order to improve the system's noise performance, the microphone should be lightly damped, which while reducing the input-refered thermal noise, unfortunately, would also result in poor frequency response and ringing due to transient signals.

One possible way to avoid the adverse effects of low damping on the dynamic response is to introduce active damping into the microphone system. The thermal noise of a microphone comes from the passive damping, usually due to viscous flow of air around the diaphragm By introducing active damping through a control feedback loop, the microphone can be designed with low passive damping to reduce thermal noise and obtain high effective damping to improve system dynamic response. Feedback control can also help expand the bandwidth of the microphone. An analysis of an active damping scheme indicates it can be effective in our design of an older generation of directional microphones incorporating parallel plate capacitive actuation, where digital control using sigma-delta modulation principle was utilized [3]. The effectiveness of active damping has also been shown in highly sensitive
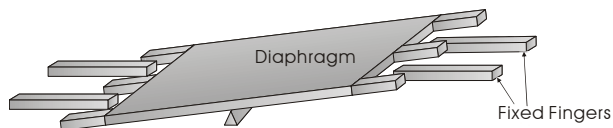
Fig. 1 Directional microphone with interdigitated comb fingers. The dimension of this microphone is $2(\mathrm{mm}) \times 1(\mathrm{mm})$

gravitational detectors [4], [5].

The directional microphone examined in the following works like a teeter-totter with interdigitated comb fingers at its ends. The diaphragm senses the external acoustic pressure gradient, and rotates around a central pivot axis. The rotation of the diaphragm is sensed optically by detecting the interference of the light that is reflected by the moving and fixed fingers [6]. This optical detection scheme has also been applied to more conventional nondirectional microphones [7]. When a voltage is applied between the movable and fixed fingers, a resulting electrostatic moment is exerted on the diaphragm, which provides the possibility of employing a force-feedback system. In the present study of the use of a feedback system, the optical transducer is modeled as a constant gain.

While the comb finger structure provides the ability to apply force feedback, there are significant challenges in using it in a control system. First, because the optical sensor provides a signal that is proportional to displacement of the movable fingers we are required to use an output feedback. Moreover, the actuation of the microphone diaphragm is through an electrostatic force, and the force is a nonlinear function of the diaphragm displacement and of the driving voltage. In addition, the unforced displacement of the diaphragm varies from device to device due to random factors in its fabrication process.

This paper focuses on formulating and analyzing an active damping control system for a directional microphone having comb fingers that addresses all the above three challenges.

The paper is organized as follows. Section II provides a mathematical description of a real silicon microphone as an example, and a feedback configuration for active damping. Section III derives a linear design model of the microphone, where both the nonlinearity of the electrostatic force transducer and the uncertainty in the unforced initial diaphragm deflection are captured in conic sectors in the system parameter space. Section IV presents the formulation and the solution of an active damping controller through the H_∞ method, where the focus of discussion is on the selection of weighting functions. Section V verifies the controller design by analyzing the performance of the closed-loop system with both the linearized model and a nonlinear Simulink model where the nonlinearity of the actuator described in Section II is implemented. Section VI concludes the paper

II. ACTIVELY DAMPED MICROPHONE MODEL

This section describes a model of the directional microphone having comb fingers as shown Fig.1, and explores the possibility of applying active damping to suppress the resonance of the diaphragm dynamics. A possible scheme for active damping is shown in Fig.2.

The microphone dynamics may be modeled as

$$I\ddot{\theta} + c\dot{\theta} + k(\theta - \theta_0) = M_r + M_e \qquad (1)$$

where I, c, and k are the moment inertia, torsional damping coefficient and torsional stiffness respectively; M_r is the moment generated by the external sound pressure gradient, M_e is the electrostatic moment generated by the comb fingers, and θ_0 is the initial unforced diaphragm rotation, formed during the device fabrication.

Since we have at our disposal a high bandwidth optical sensor that produces angular displacement measurement of the movable fingers, an active damping can be implemented by designing a feedback controller $H(s)$ with sensor gain (Volts/rad) included.

The electrostatic force F generated by each pair of comb fingers is the gradient of the electrical energy ϕ stored.

$$\phi = \frac{1}{2}CV^2 \qquad (2)$$

$$F = \frac{\partial\phi}{\partial x} = \frac{1}{2}\frac{\partial C}{\partial x}V^2, \qquad (3)$$

where x is the vertical displacement between fixed and movable fingers. C is the capacitance between each pair of fingers, V is the voltage applied, which is comprised of DC bias voltage V_0, and control voltage V_1 at the output of active damping controller.
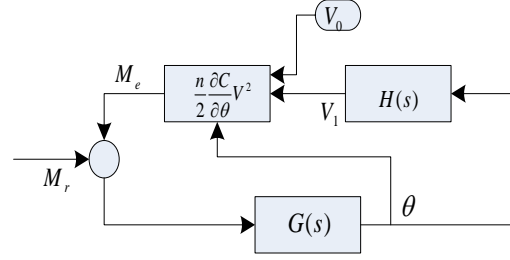

Fig. 2 A proposed active damping configuration

The total electrostatic moment generated by all the fingers is

$$M_e = \frac{n}{2}\frac{\partial C}{\partial x}V^2 L \overset{x=L\theta}{=} \frac{n}{2}\frac{\partial C}{\partial \theta}V^2, \qquad (4)$$

where L is the half length of the diaphragm, θ is diaphragm angle of rotation, and n is the total number of pairs of fingers.

The function $\frac{\partial C}{\partial \theta}$ is determined by the electric flux density distribution between the finger pairs. The conformal mapping method [8] is used to obtain its relationship to θ, as shown in Fig. 3.
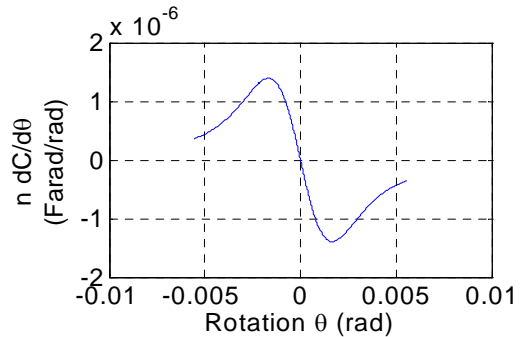
Given the expression for the electrostatic moment in

Fig. 3 $n\frac{\partial C}{\partial \theta}$ of 600 finger pairs

equation (4), the nonlinear dynamic governing equation for the system can be expressed as,

$$I\ddot{\theta} + c\dot{\theta} + k(\theta - \theta_0) = \frac{n}{2}\frac{\partial C}{\partial \theta}(V_0 + V_1)^2 + M_r \qquad (5)$$

The parameters for a specific microphone are listed in Table 1.

Table 1. Nominal parameters of the microphone

Moment Inertia I	6.2663e-15	$Kg.m^2$
Damping Coefficient c	6.5909e-12	$Kg.m/s$
Stiffness k	1.7331e-5	$Kg.m/s^2$
Half length of Diaphragm L	1e-3	m
Width of diaphragm	1e-3	m
Number of comb finger pairs n	600	

Fig. 4 Graphical solution of θ_e when the initial unforced rotation is θ_0 with a DC bias of 0.1 V

III. LINEAR DESIGN MODEL WITH CONIC UNCERTAINTIES

Referring to Fig.2, equation (5) describes the control design model consisting of microphone dynamics preceded by a nonlinear actuator. This section derives a linearized design model with uncertain parameters that capture both nonlinearities and inexact knowledge of the initial angular displacement.

The electrostatic moment presents two problems: uncertainty and nonlinearity. Suppose θ_e is the equilibrium point of the system. It is determined by

$$k(\theta_e - \theta_0) = \frac{n}{2}\frac{\partial C}{\partial \theta}\bigg|_{\theta_e} V_0^2. \tag{7}$$

A graphical solution for θ_e is shown in Fig.4. It is seen that θ_e depends on θ_0, which varies from device to device.

Let $\theta = \theta_e + \theta_d$, where θ_d is a small dynamic rotation about the equilibrium position. Expanding (5) around the equilibrium yields

$$\begin{cases} I\ddot{\theta}_d + c\dot{\theta}_d + k\theta_d + k(\theta_e - \theta_0) \\ \qquad = \frac{n}{2}\frac{\partial C}{\partial \theta}\bigg|_{\theta_e + \theta_d}(V_0 + V_1)^2. \end{cases} \tag{8}$$

Substituting (7) into (8), the system governing equation becomes

$$\begin{aligned} &I\ddot{\theta}_d + c\dot{\theta}_d + k\theta_d \\ &= \frac{n}{2}\left\{\frac{\partial C}{\partial \theta}\bigg|_{\theta_e + \theta_d}(V_0 + V_1)^2 - \frac{\partial C}{\partial \theta}\bigg|_{\theta_e} V_0^2\right\}. \end{aligned} \tag{9}$$

Applying Taylor's Theorem,

$$\begin{aligned} &I\ddot{\theta}_d + c\dot{\theta}_d + k\theta_d \\ &= \frac{n}{2}\left\{\frac{\partial^2 C}{\partial \theta^2}\bigg|_{\xi}\theta_d V_0^2 + 2\frac{\partial C}{\partial \theta}\bigg|_{\theta_e + \theta_d}V_0\left(1 + \frac{V_1}{2V_0}\right)V_1\right\} \end{aligned} \tag{10}$$

where ξ is between θ_e and $\theta_e + \theta_d$.

.

Define
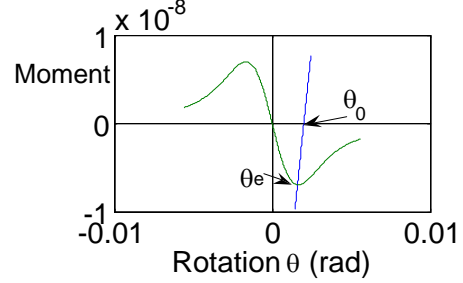
$$k_e = \frac{n}{2}\frac{\partial^2 C}{\partial \theta^2}\bigg|_{\xi} V_0^2,$$

$$k_M = n\frac{\partial C}{\partial \theta}\bigg|_{\theta_e + \theta_d}V_0\left(1 + \frac{V_1}{2V_0}\right) \tag{11}$$

A linearized incremental design model around equilibrium θ_e is obtained,

$$I\ddot{\theta}_d + c\dot{\theta}_d + (k - k_e)\theta_d = k_M V_1. \tag{12}$$

k_e becomes the equivalent electrical stiffness generated by the electrostatic moment feedback and k_M works as equivalent electrostatic gain for actuation.. Both k_e and k_M are time varying gains that are also uncertain if θ_0 is not known.

The gains can be regarded as uncertain gains, and their boundaries can be estimated for a given set of fabricated devices through the range of θ_0, θ_d, θ_e, and $\frac{\partial^2 C}{\partial \theta^2}\bigg|_{\xi}$ which is shown in Fig.5.
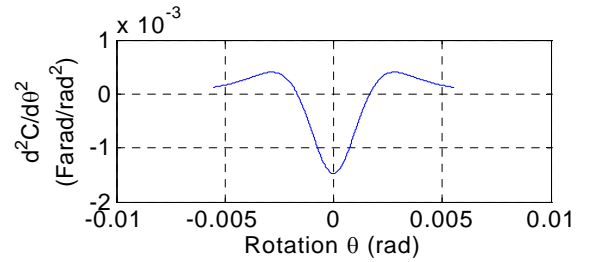

Fig. 5 $\dfrac{d^2 C}{d\theta^2}$ for 600 finger pairs

Some sample values of the boundaries are now provided. At $V_0 = 0.1$ (volt) and $\theta_e \in [1e-6, 2e-3]$ in radians, the boundaries of $\frac{\partial^2 C}{\partial \theta^2}\bigg|_{\theta_e + \eta\theta_d}$ are found to be in the range of

$[-0.00147, 0.00195]$ F/rad^2. In this case, equivalent active stiffness becomes $k_e \in [-7.36e-6, 9.77e-6]$ according to (11).

$1 + \dfrac{V_1}{2V_0}$ is bounded by $1 - \dfrac{\max|V_1|}{2V_0}$ below and $1 + \dfrac{\max|V_1|}{2V_0}$ above. Simulations of the closed-loop system upon completion of controller design, concludes the actuator gain $k_M \in [-5.568e-7, 2.048e-9]$ (Nm/Volt).

The linearization model allows the application of many design techniques for the compensator $H(s)$; this paper uses an elementary loop-shaping and H_∞ control [9].

IV. H_∞ CONTROLLER DESIGN

The Matlab routine *hinfsyn* is called for the design of compensator $H(s)$. The routine requires that the feedback interconnection of linear fractional transformation form as seen in Fig.6, where the two inputs are scaled reference input d and control input V_1, the three outputs are controlled output e_1 representing weighted angular displacement error of the diaphragm, controlled output e_2, representing weighted control voltage, and measured incremental output θ_d. The generalized plant G_{ic} in Fig. 6 is obtained by including all performance weightings in the open-loop interconnection shown in Fig.7.
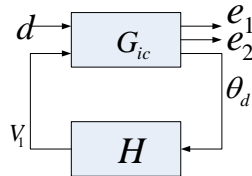

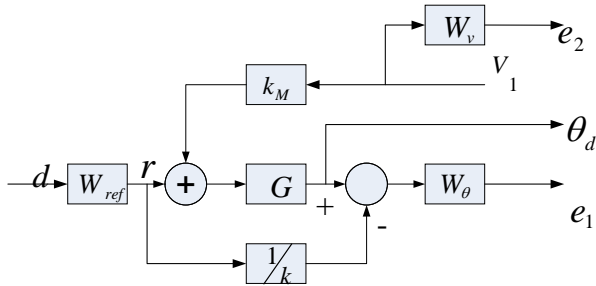*Fig. 6 Closed-loop interconnection in linear fractional transformation form*

Fig. 7 Open-loop interconnection of a two-input and three-output generalized plant with performance weightings

The generalized plant G_{ic} is given by

$$\begin{pmatrix} e_1 \\ e_2 \\ \theta_d \end{pmatrix} = \left[\begin{array}{c|c} W_{ref}W_\theta\left(G - \dfrac{1}{k}\right) & W_\theta k_M G \\ 0 & W_v \\ \hline W_{ref}G & k_M G \end{array} \right] \begin{pmatrix} d \\ V_1 \end{pmatrix}$$

$$= G_{ic}\begin{pmatrix} d \\ V_1 \end{pmatrix}$$

The idea of the H_∞ method is to find a suboptimal solution for the controller $H(s)$ that makes the H_∞ norm of the transfer function from d to (e_1, e_2) to be acceptably small. The key to a successful design is to select weighting functions that reflect the designer's intent, and to consider tradeoff among conflicting requirements.
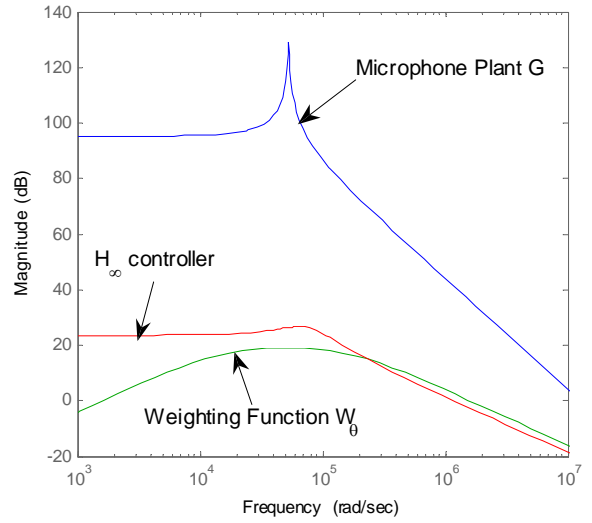

Fig. 8 Weighting function W_θ, microphone dynamics G and the designed H_∞ controller H

The first consideration in compensation is to extend the microphone operating bandwidth by pushing the occurrence of the resonant peak to outside of the frequency range of interest. This is accomplished by weighing the error of $G - \dfrac{1}{k}$ around the resonance frequency. Fig. 8 shows how the weighting function W_θ puts more weight around the resonance frequency to make error e_1 small.

$$W_\theta = \frac{6.8e-4s}{3.9e-10s^2 + 6.9e-5s + 1} \tag{14}$$

$W_v = 2$ is chosen in the final design. W_{ref} is the reference normalization weighting gain. The choice of it has tremendous effect on controller synthesis in that it scales the reference input against control input to reflect the designer's intent, and to improve the condition number of the design model. Its value is often set at the maximum of the reference input. Human speech signal is around 80dB (SPL), which has an effective moment on microphone diaphragm
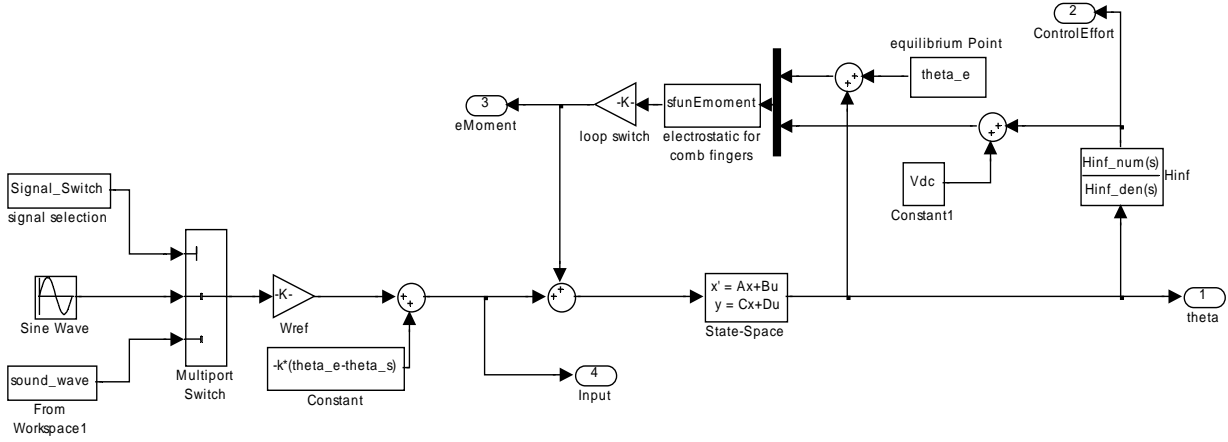
Fig.10 Simulink diagram of the closed-loop microphone

with $W_{ref} = 2.6e - 10$. The detail of the derivation of sound pressure moment can be found in Appendix A.

The closed-loop transfer function of Fig.6 is

$$ T = \begin{pmatrix} W_{ref} W_\theta \left(\dfrac{G}{1 - k_M GH} - \dfrac{1}{k} \right) \\ W_{ref} W_v \dfrac{GH}{1 - k_M GH} \end{pmatrix}. \tag{15} $$

Controller $H(s)$ is designed so that

$$ \sup_{H(s)} \|T\|_\infty < \gamma \tag{16} $$

for an acceptably small γ.

The resulting controller is given by

$$ H = 1.7e6 \frac{s - 6.712e4}{s^2 + 8.989e4s + 6.504e9}. \tag{17} $$

Fig.9 shows the closed-loop versus open-loop frequency responses for a number of parameter values within the defined boundaries.

The controller in Equation (17) has a right-hand zero, which means a non-minimum phase controller. A non-minimum phase controller may limit the close-loop bandwidth. The upper bound of closed-loop bandwidth can be decided by the following equation. [10]

$$ \omega_b \leq z \left(\alpha - \frac{1}{M_s} \right) \tag{18} $$

where ω_b is the closed-loop bandwidth; $\alpha = 1$ if loop transfer function has no right-half plane poles, which is true in our case; z is the right half-plane zero, and M_s is peak sensitivity, which is much greater than 1 when the damping ratio is small. Because the right-hand zero is greater than the peak resonance frequency (6.80e4>5.25e4) (rad/s), the controller can effectively achieve active damping without having to reduce the microphone's original bandwidth.
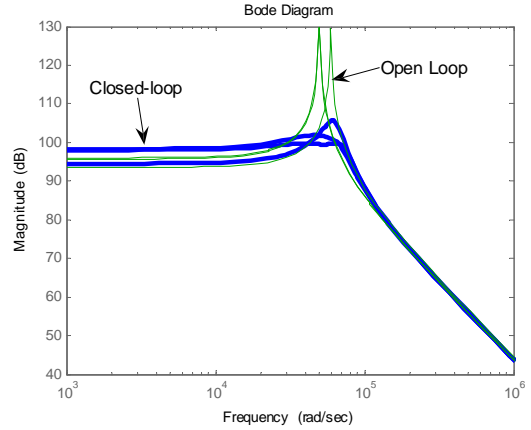

Fig.9 Open- and closed-loop frequency responses

Although the controller is designed for a particular nominal design model, it does provide certain robustness in closed-loop performance. Fig. 9 shows the open-loop and closed-loop transfer function based on different sets of parameter samples. It clearly demonstrates an effective active damping due to feedback.

V. VERIFICATION THROUGH SIMULATIONS

This section verifies the active damping design by simulating the closed-loop system with nonlinearity in the actuator included. Fig.10 shows the Simulink model of the nonlinear system.

When the reference input is a 1kHz sine wave, the response of the open loop plant continuously oscillates around the sinusoidal response due to very light damping, whereas the closed-loop response begins to follow the reference input after one period wiggling, which verifies the effect of active damping as shown in Fig.11.

The control effort shown in Fig. 12 provides some basis for determining the aforementioned range of variation for
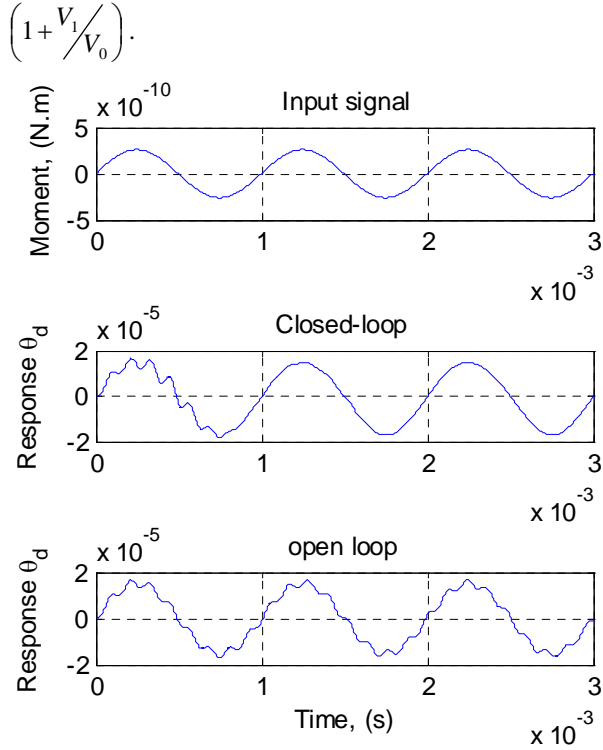
$$\left(1 + \frac{V_1}{V_0}\right).$$

Fig. 11 Response θ_d of open loop and closed-loop microphone to a 1kHz sinusoidal reference input
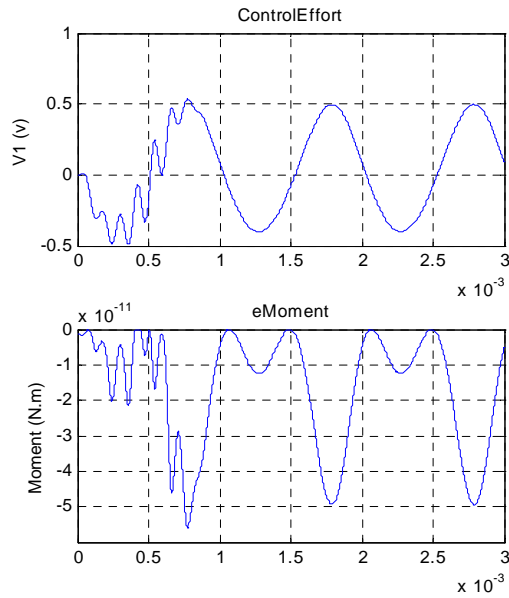

Fig.12 Control effort at the controller output and electrostatic moment output when reference signal is a 1kHz sinusoidal wave
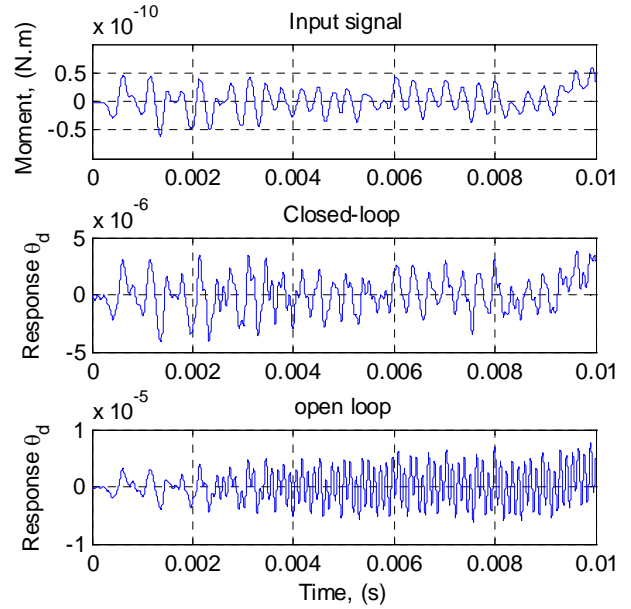

Fig. 13 Open-loop and close-loop responses to a music sound wave

Fig.13 clearly shows that ringing present in the open-loop microphone response is eliminated in the closed-loop response when a sound wave is applied at the reference input.

While setting different values of unforced diaphragm rotation θ_0, similar results can also be reached.

VI. DISCUSSION AND CONCLUSIONS

Through linearization of a nonlinear comb finger microphone, a dynamic compensator is designed that achieved the active damping of the resonance present in the open-loop microphone. The effectiveness of active damping is verified through simulations of the nonlinear microphone model. The loop-shape of the designed controller suggests a differentiation effect at the open-loop resonant peak and rolls off at high frequencies to maintain noise rejection.

This effort represents the first step in our attempt to implement a robust digital controller as part of a system-on-a-chip for the micro-machined comb finger microphone. Our immediate plan with regard to control design is to perform a thorough robustness analysis of the design, and proceed to consider other aspects of system performance, such as increased bandwidth, through formulating a robust synthesis problem. Design robustness is a necessity in low-cost mass production of the acoustic sensor.

APPENDIX A THE MOMENT GENERATED BY SOUND WAVE FOR THE DIRECTIONAL MICROPHONE

Since the microphone control design model involves two inputs, it is critical to know the magnitude range of input generated by sound pressure due to the nonlinear effect of

electrostatic actuation mechanism. The following derivation [11] shows the relationship between the pressure gradient sensed by the diaphragm of a one-dimensional directional microphone, and the moment generated. (See Fig.1). The purpose is to justify the scaling or normalization factor for the multiple inputs set up of the controller design.

Considering the plain wave pressure input,

$$p = p_0 e^{i\left(\omega t - \vec{k} \bullet \vec{r}\right)},$$
(A.1)

where $\vec{k}$ is the wave number, for 1-D problem,

$$\vec{k} \bullet \vec{r} = \left|k\right|\cos(\phi)x ,$$
(A.2)

with $\left|k\right| = \omega / c$ and c is the sound speed.

Then, the sound pressure input becomes,

$$p = p_0 e^{i\left(\omega t - \left|k\right|\cos\phi x\right)} .$$
(A.3)

The moment generated by this sound pressure

$$
\begin{aligned}
M &= \int_{-L}^{L} bx dp \\
&= \int_{-L}^{L} p_0 e^{i\left(\omega t - \left|k\right|\cos\phi x\right)} bx dx \\
&= p_0 b e^{i\omega t} \int_{-L}^{L} e^{-i\left|k\right|\cos\phi x} x dx \\
&= p_0 b e^{i\omega t} \left(\frac{i2L\cos(\left|k\right|L\cos\phi)}{\left|k\right|\cos\phi} - \frac{2i\sin(\left|k\right|L\cos\phi)}{\left|k\right|^2\cos^2\phi} \right).
\end{aligned}
$$
(A.4)

Because the common speech level does not generally exceed 80dB, $p_0 = (2e-5)\times 10^{80/20} = 0.2$ (Pascal). Therefore, the magnitude of moment generated by this signal is $\left|M\right| = 2.6e-10$ (N.m). The value is used for the scaling factor W_{ref} for the reference input in H_∞ controller design.

REFERENCES

[1] B.E. Boser and R.T. Howe, "Surface Micromachined Accelerometers", *IEEE Journal of Solid-state Circuits*, Vol 31, No.3, March, 1996
[2] R. C. Ritter and G.T. Gillies, "Classical Limit of Mechanical Thermal Noise Reduction by Feedback", *Physical Review A*, Vol 31, No. 2, Feb, 1985
[3] N.E. Wu, R. Miles, O.A. Aydin, "A digital feedback damping scheme for a micromachined directional microphone", American Control Conference, 2004, Vol. 4, pp. 3315-3320, July 2004
[4] P.F. Michelson, J.C. Price, and R.C. Taber, "Resonant-Mass Detectors of Gravitational Radiation," *Science*, Vol 237, pp. 150–156, July, 1987.
[5] A. Heidmann, P.F. Cohadon, Y. Hadjar and M. Pinard, "High-sensitivity measurement and control of thermal noise in a cavity", Gravitational Waves: Third Edoardo Amaldi Conference, pp 435-436, 2000
[6] Weili Cui, Baris Bicen, Neal Hall, Stephen Jones, F. Levent Degertekin, Ronald N. Miles, "Optical Sensing in a Directional MEMS Microphone Inspired by the Ears of the Parasitoid Fly, *Ormia ochracea*. Proceedings of MEMS 2006, Istanbul, Turkey, January 22-26, 2006.
[7] N.A. Hall and F. Levent Degertekin, "Integrated optical interferometric detection method for micromachined capacitive acoustic transducers", *Applied Physics Letters,* Vol. 80, Issue 20, pp. 3859-3861, May, 2002
[8] J.L. Andrew, Chung-yuen Hui and N.C. Tien, "Electrostatic Model for an Asymmetric Combdrive," Journal of Microelectromechanical Systems, Vol.9 No.1, pp126-134, March 2000.
[9] Kemin Zhou, J.C. Doyle,, "Essentials of Robust Control", Ch14, Prentice Hall, September, 1997
[10] Kemin Zhou, J.C. Doyle,, "Essentials of Robust Control", Ch6, Prentice Hall, September, 1997
[11] Ronald Miles, Class notes for ME622 Advanced Acoustics, 2005.